Atomistic structures of metastable and amorphous phases in ion-irradiated magnesium aluminate spinel

2002 J. Phys.: Condens. Matter 14 1237

(http://iopscience.iop.org/0953-8984/14/6/311)

INSTITUTE OF PHYSICS PUBLISHING JOURNAL OF PHYSICS: CONDENSED MATTER

J. Phys.: Condens. Matter **14** (2002) 1237–1247 PII: S0953-8984(02)31226-8

Atomistic structures of metastable and amorphous phases in ion-irradiated magnesium aluminate spinel

Manabu Ishimaru[1], **Yoshihiko Hirotsu**[1], **Ivan V Afanasyev-Charkin**[2] **and Kurt E Sickafus**[2]

[1] The Institute of Scientific and Industrial Research, Osaka University, Mihogaoka, Ibaraki, Osaka 567-0047, Japan
[2] Materials Science and Technology Division, Los Alamos National Laboratory, Los Alamos, NM 87545, USA

Received 26 November 2001
Published 1 February 2002
Online at stacks.iop.org/JPhysCM/14/1237

Abstract

Ion-beam-induced microstructures in magnesium aluminate ($MgAl_2O_4$) spinel have been examined using transmission electron microscopy (TEM). Irradiations were performed at cryogenic temperature ($\sim$120 K) on $MgAl_2O_4$ spinel single-crystal surfaces with (111) orientation, using 180 keV neon (Ne^+) ions to ion fluences ranging from 10^{16} to 10^{17} Ne^+ cm^{-2}. Cross-sectional TEM observations indicated that the $MgAl_2O_4$ spinel transforms first into a metastable crystalline phase and then into an amorphous phase under these irradiation conditions. On the basis of selected-area electron diffraction and high-resolution TEM, we concluded that Ne-ion-beam irradiation induces an ordered spinel-to-disordered rock-salt-like structural phase transformation. Atomistic structures of amorphous $MgAl_2O_4$ were also examined on the basis of atomic pair distribution functions. We compared the experimentally obtained results with previous theoretically calculated results for the metastable and amorphous phases of $MgAl_2O_4$, and discussed the validity of the proposed ion-beam-induced structural changes in $MgAl_2O_4$ spinel.

1. Introduction

The crystal structure of magnesium aluminate ($MgAl_2O_4$) spinel is assigned to the cubic space group $Fd\bar{3}m$ [1]. The conventional cubic unit cell of spinel consists of alternating octants with two different atomic arrangements (figure 1): one octant has Mg cations in tetrahedral coordination with O anions, while each adjacent octant has Al cations octahedrally coordinated with O anions. Thus, there are 32 oxygen ions, and 64 tetrahedral and 32 octahedral interstices in the unit cell. In fully ordered spinel, Mg^{2+} ions occupy eight out of the 64 available tetrahedral interstices (Wyckoff notation: 8a), with Al^{3+} ions residing in 16 of the 32 octahedral interstices (16d). The O^{2-} ions are located on the 32e sites. The oxygen parameter, which defines the deviation of the oxygen sublattice from ideal cubic close packing, is given by $u = 0.387$

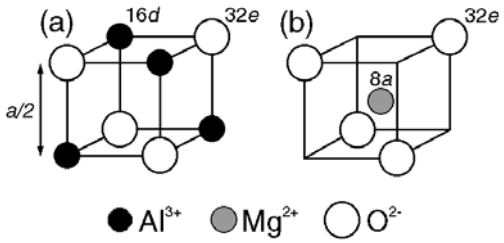

Figure 1. Atomic arrangements of (a) octahedral and (b) tetrahedral units in the normal spinel structure (lattice parameter $= a = 0.808$ nm). The various lattice sites are indicated using Wyckoff notation.

for ordered spinel (using the $\bar{4}3m$ setting for the space group). ($u_0 = 0.375$ is the oxygen parameter that would correspond to a perfect cubic close-packed anion sublattice given this choice of origin.)

Magnesium aluminate spinel compounds are attracting interest due to their potential for use as electrical insulators in future fusion reactors, due to their excellent radiation resistance. Previous studies have shown that under fast-neutron [2–4] and ion [5,6] irradiations at and above room temperatures, spinel retains crystallinity to a high damage level (up to 250 displacements per target atom (dpa) [7]). However, Yu *et al* [8] found that ion irradiation at cryogenic temperatures can induce a crystalline-to-amorphous phase transformation in $MgAl_2O_4$ spinel. Prior to amorphization, they also observed significant reduction in, or the extinction of, first-order fundamental reflections (e.g., 111 and 220) in microdiffraction patterns. It is evident from the change in the diffraction pattern that ion-beam-irradiated $MgAl_2O_4$ spinel undergoes a phase transformation to an amorphous phase through an intermediate crystalline phase. The intermediate, so-called 'metastable' crystalline phase was also observed in a nonstoichiometric spinel compound [9].

Formation of this metastable state may be a necessary prerequisite for amorphization in spinel compounds; therefore it is of great importance to identify the crystal structure of the metastable phase. Several crystal structures have been proposed for the metastable phase [10, 11]. However, interpretation of these studies is ambiguous because the amorphous-to-crystalline transition region was too thin for detailed structure analysis. We recently produced a relatively thick (∼400 nm) damage layer in order to simplify the structural analysis, and characterized the metastable crystalline phase on the basis of selected-area electron diffraction patterns [12]. The experimentally obtained results suggested that the metastable phase possesses a 'rock-salt-like' structure. However, the reflections that distinguish spinel from rock-salt are relatively weak and diffuse, but not extinct. To obtain more information on the metastable phase, we performed high-resolution transmission electron microscopy (TEM) observations in the present study. In addition to the metastable phase, amorphous structures are also examined by means of electron diffraction analyses. We compared the experimentally obtained results with previous theoretical results in order to discuss the validity of the proposed structural models for the metastable and amorphous phases in ion-irradiated $MgAl_2O_4$ spinel.

2. Experimental procedure

The single-crystalline $MgAl_2O_4$ spinel wafers (0.5 mm thick) used in this study were obtained from Linde Division, Union Carbide Corporation. The surface was normal to the [111] crystallographic axis, and polished to an optical grade finish. Ion-irradiation experiments

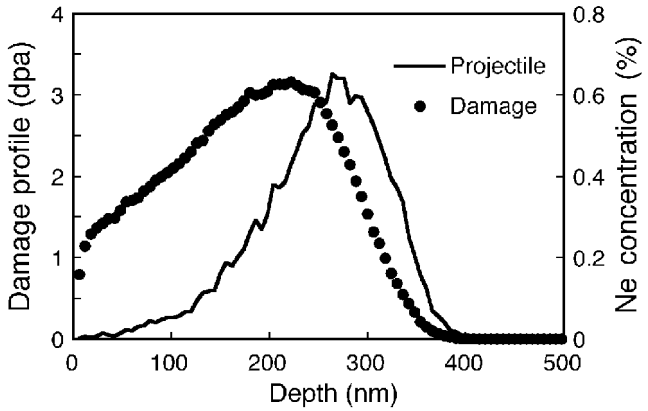

Figure 2. Monte Carlo simulation results for the number of vacancies (labelled 'dpa') created by 180 keV Ne^+ ions to a fluence of 10^{16} Ne^+ cm^{-2} in $MgAl_2O_4$ and the spatial distribution of Ne^+ projectiles as a function of target depth.

were performed at cryogenic temperature (∼120 K) with 180 keV Ne^+ ions using a 200 kV ion implanter in the Ion Beam Materials Laboratory at Los Alamos National Laboratory. The ion fluences ranged from 10^{16} to 10^{17} Ne^+ cm^{-2} and the average ion flux was maintained at $\sim 8 \times 10^{12}$ Ne^+ cm^{-2} s^{-1} during the implantations. The substrates were tilted at ∼5° from the direction of the incident ion beam in order to reduce ion-channelling effects. The sample stage was cooled to 120 K by liquid nitrogen conduction cooling. After implantation, samples were warmed to room temperature for measurement.

Cross-sectional samples for TEM observations were prepared by gluing an unirradiated $MgAl_2O_4$ sample to the surface of the irradiated $MgAl_2O_4$, cutting cross-sections of the sample (perpendicular to the irradiated surface), and using a tripod polishing technique to thin the specimens prior to ion milling with 4 keV Ar^+ ions. Irradiation-induced microstructures were examined at an incident electron energy of 300 kV using a JEOL JEM-3000F TEM, while electron diffraction patterns from an ion-beam-induced amorphous layer were obtained at an incident electron energy of 200 kV using a JEOL JEM-2010 TEM. Halo patterns were recorded on an imaging plate (Eu^{2+}-doped BaFBr) which has a higher sensitivity and wider dynamic range for electron-beam intensities compared with the commercial TEM film material [13]. The intensities of the halo patterns were analysed quantitatively in an imaging plate processor, Digital Micro-Luminography FDL 5000 (Fuji Film).

3. Results

3.1. Atomistic structures of metastable crystalline phase

Figure 2 shows the depth distribution of projectile ions and the instantaneous damage distribution generated by 180 keV Ne^+-ion bombardment of $MgAl_2O_4$ spinel. These results were obtained from Monte Carlo simulations using the TRIM code (SRIM-96) [14]. The calculations were carried out for 20 000, full-cascade ion histories, assuming a threshold displacement energy of 40 eV for all constituent elements and a lattice binding energy of 3 eV. A density of 3.58 g cm^{-3} was used for stoichiometric spinel. Simulation results in figure 2 indicate that the projectile concentration and damage peaks occur at around $R_p = 270$ and $D_p = 220$ nm, respectively. The maximum displacement damage in spinel is ∼3 dpa

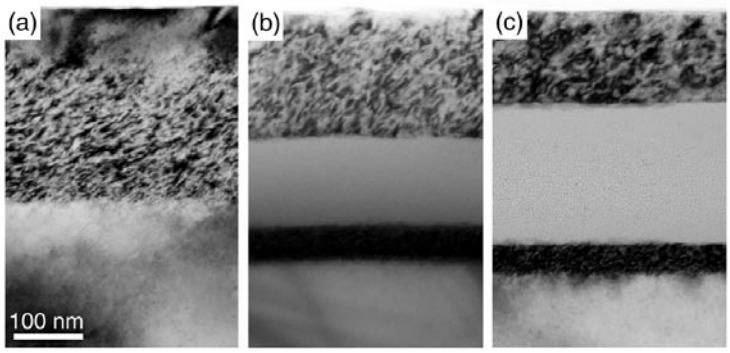

Figure 3. Cross-sectional TEM bright-field micrographs obtained from $MgAl_2O_4$ spinel irradiated with 180 keV Ne^+ ions at cryogenic temperature (∼120 K): (a) 10^{16}, (b) 5×10^{16}, and (c) 10^{17} Ne^+ cm^{-2}. The brightly imaging amorphous layer, in (b) and in (c), is surrounded by highly damaged layers (the metastable crystalline phase).

for 10^{16} Ne^+ cm^{-2} and ∼30 dpa for 10^{17} Ne^+ cm^{-2}. The thickness of sputtered material is ∼9 nm during the irradiation to a fluence of 10^{17} Ne^+ cm^{-2}. It should be noted that the vacancy distribution is asymmetrical around the damage peak maximum and the number of vacancies decreases rapidly near the end of the range of the projectile.

Figure 3 shows bright-field TEM images obtained from samples ion irradiated to doses of (a) 10^{16}, (b) 5×10^{16}, and (c) 10^{17} Ne^+ cm^{-2}. The samples were aligned near a $[1\bar{1}0]$ orientation to obtain the images of figure 3. No continuous amorphous layer is formed in figure 3(a), although there is a distinct damaged layer between 80 and 280 nm. Electron diffraction observations revealed that no amorphous phase exists in the defected layer in figure 3(a). On the other hand, a continuous buried amorphous layer is formed in specimens subjected to ion fluences of $\geqslant 5 \times 10^{16}$ Ne^+ cm^{-2}, and the amorphous region grows in size with increasing ion fluence (see figures 3(b) for 130 nm and (c) for 200 nm). Previous investigations using xenon ions showed that amorphization of $MgAl_2O_4$ is initiated by a dose of ∼25 dpa [15], which is comparable with the observations in the present study.

Significant damage is observed in regions adjacent to the amorphous layer. The upper portion of the damage regions consists of large defects. By contrast, small defects congregate at the lower portions of the damage region and the defect concentrations are larger than in the upper damage regions. The difference between the upper and lower defected layers can be attributed to the spatial distribution of the ion-beam-induced damage shown in figure 2. It is generally observed that for ion-beam irradiation, the lower-damage edge moves very little with increasing ion fluence. In the ion-irradiated $MgAl_2O_4$ spinel, however, its position changes drastically as a consequence of amorphization (cf figures 3(a) and (b)), suggesting that the large-volume expansion occurs due to crystalline-to-amorphous phase transformation. A previous theoretical study [16] predicted that the amorphous structure has a volume significantly larger than that of normal spinel, in agreement with the present experimental study.

Selected-area electron diffraction (SAED) patterns obtained from spinel substrate regions in different orientations are shown in figure 4, labelled (a), (b), and (c). The corresponding SAED patterns from the defected crystal regions in spinel samples irradiated to a fluence of 10^{16} Ne^+ cm^{-2} are also shown in figure 4, labelled (a′), (b′), and (c′). These SAED patterns were taken from uniform-thickness regions to minimize effects of sample thickness on the diffracted intensities. The electron beam was incident along $[1\bar{1}0]$ in figures 4(a), (a′), along $[1\bar{1}2]$ in figures 4(b), (b′), and along $[12\bar{3}]$ in figures 4(c), (c′). In SAED patterns obtained

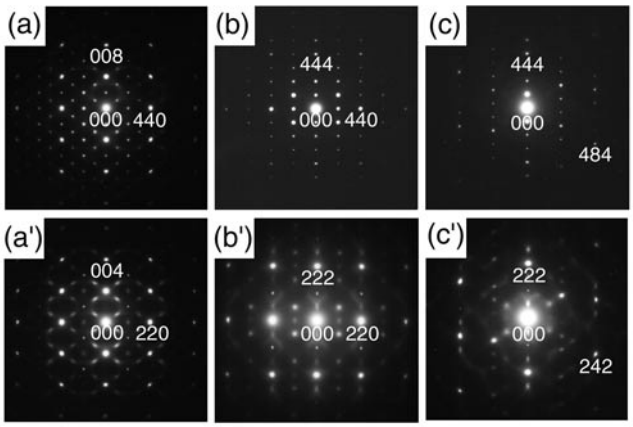

Figure 4. SAED patterns obtained from ((a)–(c)) spinel (substrate) and ((a′)–(c′)) the defected crystal layers in spinel crystals irradiated to a fluence of 10^{16} Ne^{+} cm^{-2}. Each SAED pair represents a different crystal orientation: (a), (a′) $(1\bar{1}0)$; (b), (b′) $(1\bar{1}2)$; and (c), (c′) $(12\bar{3})$ reciprocal-lattice planes. The *hkl* indices in (a)–(c) are based on the 0.808 nm repeat distance for the conventional spinel unit cell. The *hkl* indices in (a′)–(c′) are specified assuming a 0.404 nm repeat distance for the cubic unit cell of the metastable phase.

from ion-damage layers (figures 4(a′)–(c′)), the intensities of first-order fundamental lattice reflections are reduced significantly. Moreover, the intensity in these reflections is diffused. By contrast, second-order reflections in these SAED patterns remain strong and sharp. These observations suggest that $MgAl_2O_4$ transforms to a crystal structure distinct from spinel prior to amorphization.

From the symmetry of these diffraction patterns (as well as others not shown here for different crystallographic orientations), we have determined that the structure of the irradiated layer is cubic (as is the structure of spinel), but the repeat unit of the structure is half that of spinel. The *hkl* indices in figures 4(a)–(c) are based on the 0.808 nm repeat distance for the conventional spinel unit cell. On the other hand, the *hkl* indices in figures 4(a′)–(c′) are specified assuming a 0.404 nm repeat distance for the cubic unit cell of the metastable phase. The SAED patterns of the metastable phase apparently reveal that *all even hkl* reflections (e.g., 222 for the altered cubic unit cell) possess strong intensity, while *all odd hkl* reflections (e.g., 111) are weak. A 'rock-salt-like' structure was found to best fit the SAED observations in figures 4(a′)–(c′) [12], suggesting that ion-beam irradiation of $MgAl_2O_4$ induces an ordered spinel-to-disordered rock-salt-like structural phase transformation. This is a disordered structure in which the anion sublattice maintains a 'pseudo'-cubic close-packed arrangement (as in spinel), while the cations occupy randomly the octahedral lattice interstices. All tetrahedral interstices are vacant in this model. Soeda *et al* [17] examined the atomic configurations of ion-irradiated spinel compounds using the electron-channelling-enhanced x-ray microanalysis and large-angle convergent-beam electron diffraction. They found that ion irradiation causes displacements of cations from the tetrahedral sites to the octahedral sites and further enrichment of vacancies on the tetrahedral sites. This result is qualitatively consistent with the present experiments.

The ordered spinel-to-disordered rock-salt-like structural phase transformation was also confirmed by high-resolution TEM. Figure 5 shows high-resolution TEM micrographs obtained from (a) the unirradiated substrate and (b) the damage layer of the sample irradiated to a fluence of 10^{16} Ne^{+} cm^{-2}. These micrographs were obtained with the electron beam aligned

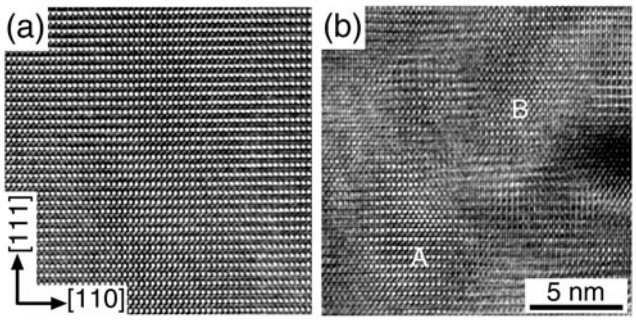

Figure 5. Cross-sectional high-resolution TEM micrographs of (a) the unirradiated spinel substrate and (b) the ion-beam-induced damage layer in a sample irradiated to a fluence of 10^{16} Ne^{+} cm^{-2}. These micrographs were obtained with the electron beam oriented along the $[1\bar{1}2]$ direction with respect to the unirradiated substrate.

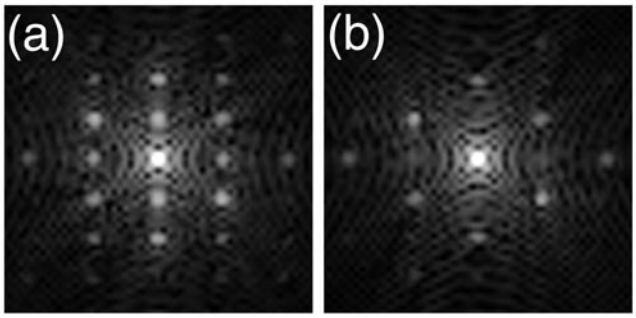

Figure 6. Diffractograms obtained by FFT from regions A and B in the high-resolution TEM image of figure 5(b).

along $[1\bar{1}2]$ with respect to the $MgAl_2O_4$ spinel substrate. Two distinct atomic arrangements, indicated by A and B, are apparent in figure 5(b). The lattice pattern of region A possesses a doubly redundant periodicity along the [111] direction, the same as that of the substrate (figure 5(a)). On the other hand, the double periodicity fades and disappears in region B. Diffractograms obtained by fast Fourier transformation (FFT) from crystallites A and B are shown in figures 6(a) and (b), respectively. The FFT diffractogram of figure 6(a) corresponds to the reciprocal-lattice plane of $MgAl_2O_4$ spinel oriented along $[1\bar{1}2]$ (i.e., equivalent to the unirradiated substrate orientation), while the first-order reflections in figure 6(b) are significantly diminished in intensity. The features of the FFTs in figures 6(a) and (b) are in good agreement with the SAED pattern of spinel (figure 4(b)) and the metastable phase (figure 4(b′)), respectively. In the diffraction patterns of figure 4, the reflections that distinguish spinel from rock-salt are relatively weak and diffuse, but not extinct. This is because there is always retained spinel (e.g., region A in figure 5(b)) in the metastable phase, interspersed with regions of rock-salt (B).

3.2. Atomistic structures of amorphous phase

We examined atomistic structures of an ion-beam-induced amorphous layer by electron diffraction techniques. The details of the electron diffraction analysis are described

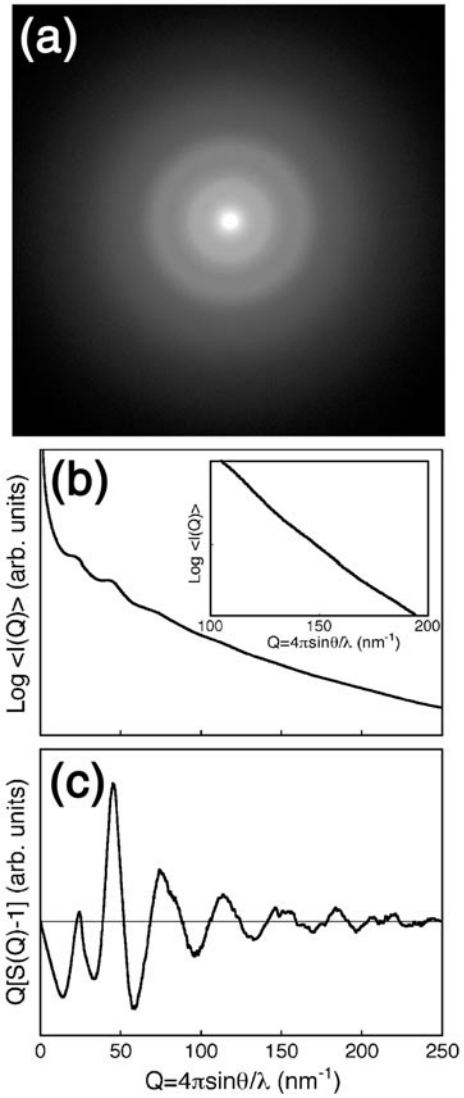

Figure 7. The electron diffraction pattern and its intensity profile obtained from the amorphous layer induced by neon implantation into $MgAl_2O_4$ spinel. (a) Halo patterns obtained from the buried amorphous layer, (b) the averaged intensities $\langle I(Q)\rangle$, and (c) the reduced interference function $Q[S(Q)-1] = Qi(Q)$.

elsewhere [18, 19]. Recrystallization occurred during observations at an incident electron energy of 300 kV using a JEOL JEM-3000F equipped with a field emission gun. Therefore, we observed the amorphous regions using a JEOL JEM-2010 equipped with a conventional LaB_6 filament, as described in section 2. Figure 7 shows an example of electron diffraction patterns obtained from the buried amorphous layer. The incident electron beam was focused to $\sim$100 nm diameter. We took some electron diffraction patterns with different exposure times, and confirmed that their intensity profiles are almost the same. That is, the electron-beam damage in the present material during the exposures is negligible. The intensities of the halo patterns in figure 7(a) were analysed quantitatively at high and low sensitivities in

a Digital Micro-Luminography FDL 5000. Averaged intensities $\langle I(Q)\rangle$ at Q in the radial direction in reciprocal-lattice space were obtained up to the scattering vector $Q = 4\pi \sin\theta/\lambda = 250\,\mathrm{nm}^{-1}$, where θ and λ are the half-scattering angle and the electron wavelength, respectively (figure 7(b)). The camera length was corrected using Bragg reflections from the $MgAl_2O_4$ spinel substrate.

In order to determine the atomic pair distribution function $g(r)$ with a sufficient accuracy, the interference function $i(Q) = S(Q) - 1$, where $S(Q)$ is the structure factor for the electron diffraction intensities, must be obtained as correctly as possible. The function $i(Q)$ can be obtained by subtracting a smooth cubic spline curve for background $I_{BG}(Q)$ which penetrates through the halo intensity ripples of $\langle I(Q)\rangle$ along Q. The reduced radial distribution function $G(r) = 4\pi r\rho_0[g(r) - 1]$ (ρ_0 is the average number density of atoms) was calculated by the Fourier transformation of the product of $Qi(Q)$ and a window function. If $I_{BG}(Q)$ is not correctly drawn, the range of radial distance between the rising edge of the first peak and $r \sim 0$ of $G(r)$ does not become a straight line, but a large ripple exists. Therefore, the correction of $I_{BG}(Q)$ is repeated until the extra ripple of $G(r)$ disappears. Figure 7(c) shows an example of the $Qi(Q)$ obtained. Very weak intensity profiles up to high scattering angles as high as $Q \sim 200\,\mathrm{nm}^{-1}$ can be recorded well above the background intensity level of the imaging plate.

The $g(r)$ obtained from the amorphous layer of figure 3(c) is displayed in figure 8. Electron diffracted intensities are highly susceptible to modification by dynamical effects such as multiple scattering. In order to optimize structural analyses of amorphous regions in irradiated $MgAl_2O_4$ by means of electron diffraction, we obtained electron diffraction patterns from thin-foil regions that were as thin as possible. The first and second peaks are centred at ∼0.18 and ∼0.21 nm, respectively. It should be noted that a shoulder appears in the large-r region of the first peak in figure 8. From the attractive interaction between the cation and anion and the ratio of Mg and Al atoms, the first peak and its shoulder are assignable to Al–O and Mg–O bonds, respectively. The locations of the peaks do not agree with the bond lengths between ions that are close neighbours in the normal spinel, marked with the arrows in the upper part of figure 8 (Mg–O: 0.193 nm; Al–O: 0.194 nm; O–O: 0.260, 0.289, 0.316 nm; Mg–Al: 0.337 nm; and Al–Al: 0.289 nm within the distance of 0.4 nm). That is, the Al–O bond length (∼0.18 nm) becomes smaller than that in the normal spinel structure, whereas the Mg–O bond length (∼0.21 nm) becomes large. Amorphous structures proposed by Chen *et al* [16] reproduce well the experimentally obtained functions $g(r)$ (figure 8).

4. Discussion

The crystallographic description of the spinel-to-rock-salt-like structure phase transformation is as follows:

$(Mg_{1.0})_{8a}(\bullet_{1.0})_{8b,48f}[Al_{1.0}]_{16d}[\bullet_{1.0}]_{16c}(O_{1.0})_{32e}$
ordered spinel ($Fd\bar{3}m$; origin at $\bar{4}3m$)

$$\xrightarrow{\text{first transformation description}} (\bullet_{1.0})_{8a,8b,48f}[Mg_{0.25}Al_{0.50}\bullet_{0.25}]_{16d}[Mg_{0.25}Al_{0.50}\bullet_{0.25}]_{16c}(O_{1.0})_{32e}$$
metastable phase ($Fd\bar{3}m$; origin at $\bar{4}3m$)

$$\xrightarrow{\text{alternate transformation description}} (\bullet_{1.0})_{8c}[Mg_{0.25}Al_{0.50}\bullet_{0.25}]_{4a}(O_{1.0})_{4b}$$
metastable phase ($Fm3m$; origin at $m3m$),

where • represents a vacancy. The first transformation description above is based on the doubly redundant 0.808 nm unit cell. The second transformation description refers to the 0.404 nm rock-salt unit cell. In the ordered spinel structure, one in eight of the tetrahedral

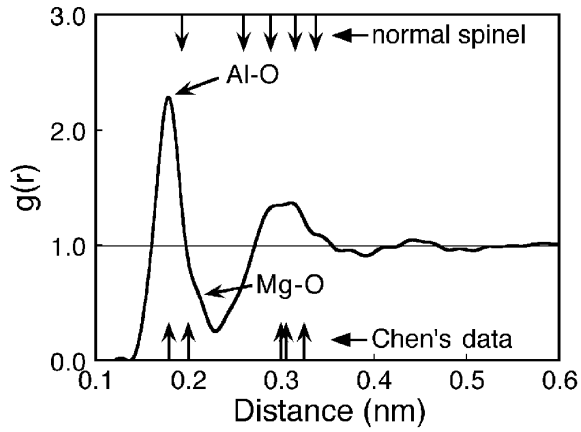

Figure 8. An atomic pair distribution function $g(r)$ extracted by the Fourier transformation of figure 7(c). The arrows at the top and bottom indicate the atomic distances in normal spinel and amorphous $MgAl_2O_4$, respectively, calculated by Chen *et al* [16]. The $g(r)$ obtained is in excellent agreement with the calculated peak positions for amorphous $MgAl_2O_4$ (Mg–O: 0.200 nm; Al–O: 0.179 nm; O–O: 0.300 nm; Mg–Al: 0.306 nm; and Al–Al: 0.325 nm within the distance of 0.4 nm).

interstices (8a, 8b, 48f) are occupied. In the disordered rock-salt phase, all tetrahedral sites are empty (8c in the second description). Octahedral interstices are occupied at random in the disordered rock-salt structure, while the anion sublattice remains more or less undisturbed by the transformation.

Lattice energy calculations for some of the model structures lend support to the spinel-to-rock-salt transformation proposed here. Chen *et al* [16] performed total-energy calculations for various $MgAl_2O_4$ metastable phase models, using a Born-like description of an ionic lattice and the shell model to describe the polarization of ions. Several computed results for the rock-salt structure are corroborated by experimental observations. For instance, the computed rock-salt structure possesses a molecular volume similar to spinel (6% contraction), while other model structures have much larger calculated molecular volumes (15–30% expansion relative to spinel). Experimental observations indicate that the volume change upon formation of the metastable phase is small (only 3–5% expansion) [9]. Also, the calculated elastic modulus for the rock-salt phase was found to be larger (by 28%) than the modulus of spinel, while calculations for all other model structures (except an inverse spinel structure, in which the characteristic spinel superlattice is maintained) indicate that the elastic modulus is decreased compared to spinel. Using nanoindentation techniques, Devanathan *et al* [20] and Yu *et al* [15] found that the elastic modulus of ion-irradiated spinel increases by 10–15% upon formation of the metastable phase. This concurs with a rock-salt-like transformation.

The high-resolution TEM micrograph of figure 5(b) provides additional insight into the metastable phase in ion-irradiated $MgAl_2O_4$ spinel. The migration of ion-beam-induced defects is suppressed at low temperatures, with the result that the metastable crystalline phase with a rock-salt-like structure is formed heterogeneously in the damage layer. On the other hand, a highly inverted spinel phase is observed in $MgAl_2O_4$ spinel irradiated at high temperatures [7]. These results suggest that the formation of the metastable phase requires the damage accumulation without long-range defect diffusion. Chen *et al* [16] proposed an example of a possible amorphization process for ion-irradiated $MgAl_2O_4$. They indicated that when spinel is heavily irradiated, it is energetically more favourable to transform to the

amorphous phase through the generation of many tetragonal rock-salt metastable structures. Atomistic structures of the metastable and amorphous phases of $MgAl_2O_4$ induced by ion irradiation are in good agreement with those obtained by the lattice energy calculations, suggesting the validity of the amorphization mechanisms of ion-irradiated $MgAl_2O_4$ spinel proposed by Chen *et al*.

5. Conclusions

Atomistic structures of metastable and amorphous phases in ion-irradiated $MgAl_2O_4$ spinel were examined in detail using TEM. Prior to amorphization, SAED observations indicate that first-order fundamental Bragg reflections are significantly diminished in intensity. This is indicative of a transformation into a different crystal structure, the so-called metastable phase. The irradiated crystalline phase possesses the same FCC Bravais lattice as spinel, but its lattice parameter is reduced from spinel's lattice parameter of 0.808 to about 0.4 nm. It was confirmed that the features of SAED patterns obtained from the irradiation-induced damage layer correspond to those of the rock-salt structure in which all cations reside randomly on octahedral interstices within a 'pseudo'-cubic close-packed oxygen-anion sublattice. This result suggests that an ordered spinel-to-disordered rock-salt-like structural phase transformation in $MgAl_2O_4$ is induced by ion-beam irradiation. Atomic pair distribution functions indicate that in amorphous $MgAl_2O_4$, the Al–O bond length becomes smaller than that in the normal spinel structure, whereas the Mg–O bond length become large. The atomistic structures of the metastable and amorphous phases obtained here are in good agreement with those determined by theoretical calculations, suggesting the validity of the proposed ion-beam-induced structural changes in $MgAl_2O_4$ spinel.

Acknowledgments

We would like to thank J R Tesmer, M G Hollander and C R Evans for their assistance with ion implantations and T Ohkubo for his development of computer code for electron diffraction analysis. We are also grateful to Professor Matsumura for his fruitful comments. This work was sponsored by the US Department of Energy, Office of Basic Sciences, Division of Materials Sciences and Special Coordination Funds for Promoting Science and Technology on 'Nanohetero Metallic Materials' from the Science and Technology Agency and a Grant-in-Aid for Scientific Research from the Ministry of Education, Science, Sports and Culture, Japan. MI also acknowledges partial support from the Foundation of Kyushu Industrial Technology Centre (KITEC) for his research abroad.

References

[1] For example see Wyckoff R W G 1965 *Crystal Structure: Inorganic Compounds* $R_x(MX_4)_{y'}$, $R_x(M_nX_p)_{y'}$ *Hydrates and Ammoniates* vol 3 (New York: Wiley)
[2] Clinard F W, Hurley G F and Hobbs L W 1982 *J. Nucl. Mater.* **108–9** 655
[3] Tucker D S, Zocco T, Kise C D and Kennedy J C 1986 *J. Nucl. Mater.* **141–3** 401
[4] Nakai K, Fukumoto K and Kinoshita C 1992 *J. Nucl. Mater.* **191–4** 630
[5] Knight P A, Jenkins M L and Pells G P 1989 *Mater. Res. Soc. Symp. Proc.* **152** 135
[6] Zinkle S J 1989 *J. Am. Ceram. Soc.* **72** 1343
[7] Sickafus K E, Larson A C, Yu N, Nastasi M, Hollenberg G W, Garner F A and Bradt R C 1995 *J. Nucl. Mater.* **219** 128
[8] Yu N, Sickafus K E and Nastasi M 1994 *Phil. Mag. Lett.* **70** 235
[9] Sickafus K E, Yu N, Devanathan R and Nastasi M 1995 *Nucl. Instrum. Methods* B **106** 573

[10] Devanathan R, Sickafus K E, Yu N and Nastasi M 1995 *Phil. Mag. Lett.* **72** 155
[11] Wang L W, Gong W L, Bordes N, Ewing R C and Fei Y 1995 *Mater. Res. Soc. Symp. Proc.* **373** 407
[12] Ishimaru M, Afanasyev-Charkin I V and Sickafus K E 2000 *Appl. Phys. Lett.* **76** 2556
[13] Mori N, Oikawa T, Harada Y and Miyahara J 1990 *J. Electron Microsc.* **39** 433
[14] Ziegler J F, Biersack J P and Littmark U 1985 *The Stopping and Range of Ions in Solids* (New York: Pergamon)
[15] Yu N, Devanathan R, Sickafus K E and Nastasi M 1997 *J. Mater. Res.* **12** 1766
[16] Chen S P, Yan M, Gale J D, Grimes R W, Devanathan R, Sickafus K E, Yu N and Nastasi M 1996 *Phil. Mag. Lett.* **73** 51
[17] Soeda T, Matsumura S, Hayata J and Kinoshita C 1999 *J. Electron Microsc.* **48** 531
[18] Ohkubo T, Hiroshima T, Hirotsu Y, Inoue A and Oikawa T 2000 *Mater. Trans. JIM* **41** 1385
[19] Hirotsu Y, Ishimaru M, Ohkubo T, Hanada T and Sugiyama M 2001 *J. Electron Microsc.* at press
[20] Devanathan R, Yu N, Sickafus K E and Nastasi M 1996 *J. Nucl. Mater.* **232** 59